Engineered Science
DOI: https://dx.doi.org/10.30919/es1477

Electrically Insulating Composite Films with Excellent Electromagnetic Interference Shielding Performance Enabled by Multilayer Structure

Lei Wang,[1, 3,*] Li Lang,[1] Weining Ren,[1] Zelong Yang,[1] Tiantian Gao,[1] Zhongguo Zhao,[1,*] Mohamed Kallel[4] and Yuezhou Liu[2,*]

Abstract

Insulating polymer-based electromagnetic interference (EMI) shielding composites play a pivotal role in electronic packaging and flexible electronics. In this work, insulating poly(3,4-ethylene dioxythiophene):polystyrene sulfonic acid (PEDOT:PSS)/bacterial cellulose (BC) EMI shielding composite films with excellent mechanical properties and superior flexibility are prepared by layer-by-layer assembly. The PEDOT:PSS/BC composite films present excellent electrical insulation properties, mechanical properties and chemical stability. When the mass fractions of PEDOT:PSS are 50 wt%, the PEDOT:PSS/BC composite films exhibit volume resistivity as high as 2.0×10^6 Ω·cm and EMI shielding effectiveness (SE) of 72 dB in the X-band (8.2-12.4 GHz), and they can maintain efficient EMI shielding performance under various harsh conditions (high temperature, low temperature and ultrasonication). Furthermore, the PEDOT:PSS/BC composite films possess excellent flexibility, mechanical properties, and long-term durability (harsh chemical environments and severe mechanical wearing). This work proposes a facile strategy to design insulating polymer-based EMI shielding composite films with excellent mechanical properties and superior flexibility, which shows great potential for applications in electronic packaging, flexible electronic devices, aeronautics and astronautics.

Keywords: Electromagnetic interference shielding; Electrical safety; PEDOT:PSS; Electrical insulation.
Received: 29 March 2023; Revised: 15 April 2025; Accepted: 24 April 2025.
Article type: Research article.

1. Introduction

With the rapid development of electronic devices and wireless communication technology, the ensuing electromagnetic pollution is becoming increasingly serious,[1,2] which poses a potential threat to the normal operation of electronic devices and human health.[3,4] In order to solve this problem, the development of lightweight and flexible of high-performance electromagnetic interference (EMI) shielding materials has become an important research direction in the field of electronic packaging.[5-7]

Conventional metal-based EMI shielding composites demonstrate high conductivity (σ) and remarkable EMI shielding performance.[8-10] However, they face limitations including high density and poor flexibility.[11,12] Currently, polymer-based conductive composites have drawn much attention due to their lightweight,[13-15] stable chemical properties and adjustable properties.[16-18] Among them, as an typical conductive polymer, poly(3,4-ethylene dioxythiophene):polystyrene sulfonic acid (PEDOT:PSS) includes positively charged electrically conductive conjugated PEDOT and negatively charged insulating PSS.[19,20] The composition ensures the stability of the positively charged conjugated PEDOT in water and other polar solvents.[21-23] Moreover, PEDOT:PSS exhibits superior σ and biocompatibility, garnering significant interest from scholars in EMI shielding.[24,25] Pritom *et al*.[26] prepared PEDOT:PSS films by casting method followed by annealing treatment, and

[1] *School of Chemistry and Environment Science, Shaanxi University of Technology, Hanzhong, Shaanxi, 723001, China*
[2] *Xi'an Modern Chemistry Research Institute, Xi'an, Shaanxi, 710065, China*
[3] *Shaanxi Key Laboratory of Macromolecular Science and Technology, School of Chemistry and Chemical Engineering, Northwestern Polytechnical University, Xi'an, Shaanxi, 710072, China*
[4] *Department of Physics, College of Science, Northern Border University, Arar, 100026, Saudi Arabia*
**Email:* mxera@snut.edu.cn, minishiguang@126.com (L. Wang); zhaozhongguo@snut.edu.cn (Z. Zhao), 21637032@zju.edu.cn (Y. Liu)

the EMI shielding effectiveness (SE) was 20 dB at 40 μm thick. However, the intrinsic brittleness and low ductility of PEDOT:PSS films, attributed to their rigid conjugate structure, result in a lack of flexibility and poor mechanical properties, which significantly constrained the advancement of PEDOT:PSS films in EMI shielding. Scholars attempt to enhance the mechanical properties of PEDOT:PSS films by compositing polymers such as aramid nanofiber (ANF),[27,28] polyvinyl alcohol (PVA),[29] bacterial cellulose (BC),[30] phenylene-2,6-benzobisoxazole (PBO),[31-33] cellulose nanofibers (CNF),[34-36] and polyimide (PI).[37] Shen *et al*.[38] prepared Janus bilayer-structured ANF/MXene-PEDOT:PSS films by a two-step vacuum-assisted filtration technique. The EMI SE of ANF/MXene-PEDOT:PSS Janus films were 45 dB at 25 μm thick. Liu *et al*.[39] fabricated caffeic acid-modified multi-walled carbon nanotubes (C-MWCNT)/PEDOT:PSS/PI composite films (CPFs) using a simple layer-by-layer deposition method with a "reinforced concrete" structure, and the EMI SE of CPFs reached 32 dB at 47 μm thick. Luo *et al*.[40] prepared carbon nanotubes (CNT) /CNF/PEDOT:PSS films by vacuum-assisted filtration. The insulating CNF interlayer separates the two conductive layers and keeps them relatively independent of each other. With a thickness of 0.14 mm, the EMI SE of CNT/CNF/PEDOT:PSS film was up to 60 dB.

However, simply improving the mechanical properties and EMI SE of the PEDOT:PSS composite films have gradually failed to meet the multifunctionalization requirements in practical applications.[41,42] For example, in electronic packaging, the EMI shielding composites are required to possess high EMI SE, excellent mechanical properties,[43] electrical insulation properties and chemical stability for safety and performance stability of equipment.[44-46] Accordingly, Zhou *et al*.[47] proposed a theoretical model of insulating EMI shielding structure, which breaks the traditional concept that it was difficult for electrical insulating materials to have efficient EMI shielding performance and opens up a new way for the design of insulating EMI shielding polymer composites. Li *et al*.[48] fabricated CNF@boron nitride nanosheet (BNNS)/silver nanowires (AgNW)/BC composite films with excellent insulating properties by a simple vacuum-assisted filtration technique. When the mass fraction of AgNW was 4.76 wt%, the EMI SE reached 49 dB. The multilayer structural has proved to be an effective strategy for design of EMI shielding composites with excellent electrical insulation and mechanical properties.[49]

BC, as a natural biopolymer, possesses high purity, satisfactory biocompatibility and superior mechanical properties,[50,51] demonstrating great potential for applications in EMI shielding and flexible electronics.[52-54] In this work, insulating PEDOT:PSS/BC EMI shielding composite films with excellent mechanical properties and superior flexibility are prepared by layer-by-layer assembly. This multilayer structure endows the PEDOT:PSS/BC composite films with superior EMI shielding performance, mechanical properties and chemical stability. This work provides a facile strategy for the design of flexible insulating multifunctional polymer-based composite films, with broad applications in the fields such as electronic packaging, flexible electronic devices, aeronautics and astronautics.

2. Materials and method

2.1 Main raw materials

Bacterial cellulose (BC) is supplied by Xi'an Qiyue Biotechnology Co., Ltd (China). PEDOT:PSS is purchased from Shanghai one organic photoelectric materials Co., Ltd (China). sodium hydroxide (NaOH, 97%) and concentrated HCl are both received from Shanghai Macklin Inc. N, N-Dimethylformamide (DMF) is purchased from Tianjin Fuyu Fine Chemical Co., Ltd (China).

2.2 Preparation of BC/PEDOT:PSS films

The initial BC layer is obtained through the evaporation of BC solution (0.6 wt%) at 80 ºC. Subsequently, the PEDOT:PSS solution (1 wt%) and BC solution are added dropwise alternately and evaporated to obtain multilayer PEDOT:PSS/BC composite films with isolated conductive networks. The dosage of PEDOT:PSS are 1 mL, 2 mL, 3 mL, 4 mL, and 5 mL, and the dosage of BC solution are 7.5 mL, 6.6 mL, 5.8 mL, 5 mL, and 4.1 mL, respectively. The total mass of PEDOT:PSS/BC composite film is 200 mg. Finally, the prepare BC/PEDOT:PSS composite films are subjected to a cold-pressing treatment (1 MPa, 12 hrs) at 45 ºC to optimize the PEDOT:PSS/BC composite films properties.

2.3 Characterizations

X-ray diffraction (XRD) of the samples was collected on a Shimadzu-7000 type X-ray diffraction (λ = 0.154 nm, Shimadzu, Japan). X-ray photoelectron spectroscopy (XPS) analyses of the samples were obtained on a PHI5400 device (PE Co., England). Scanning electron microscope (SEM) images of the samples were obtained on Hitachi SU8010 field emission scanning electron microscope at an accelerating voltage of 5 kV (Hitachi Corp., Japan). Electrical conductivities of the samples were analyzed by RTS-8 (Guangzhou Four Probes Technology Co., China). Surface resistivity of the samples was measured by AS982 (Dongguan Wan Chuang Electronic Products Corp., China). EMI shielding performance of the samples was measured by a MS4644A Vector Network Analyzer instrument (Anritsu Co., Japan), which used the wave-guide method in the X-band frequency range according to ASTMD5568-08, and the corresponding specimen dimension was 22.86 mm × 10.16 mm × 3.00 mm. Mechanical properties of the samples were tested by Instron Bluehill LE type microcomputer controlled electronic universal testing machine according to ISO 1184-1983 (Instron Co., America) at a rate of 5 mm/min.

3. Results and discussion

3.1 Preparation of PEDOT:PSS/BC composite films

Figs. 1a and b are the structure formula of PEDOT:PSS and structure model of BC. Fig. 1c is a schematic diagram of the structure for PEDOT:PSS/BC composite film. Fig. 1d illustrates the schematic diagram for the fabrication of the PEDOT:PSS/BC composite films. The initial BC layer is obtained through the evaporation of BC solution at 80 ºC. Subsequently, the PEDOT:PSS solution and BC solution are added dropwise alternately and evaporated to obtain multilayer PEDOT:PSS/BC composite films with isolated conductive networks. Fig. 1e illustrates that the contact angle of the PEDOT:PSS/BC composite film is 38.1º, indicating that the PEDOT:PSS/BC composite films are hydrophilic and can be tightly fitted to the protected object. Fig. 1f shows the digital photo of the PEDOT:PSS solution, which appears in light blue and exhibits favorable stability and homogeneity after placing for a long time. Fig. 1g demonstrates the excellent flexibility of the PEDOT:PSS/BC composite films, which can be manipulated freely, including being folded into complex shapes like paper airplanes without any cracks.

3.2 Chemical structure of PEDOT:PSS/BC composite films

Fig. 2a shows the X-ray diffraction (XRD) patterns of BC, PEDOT:PSS and the PEDOT:PSS/BC composite films. The BC exhibits three diffraction peaks at 2θ = 14.6º, 16.9º and 22.6º, corresponding to the (101), (010) and (002) crystal planes of cellulose, indicating a typical cellulose crystal structure of type I_α. The PEDOT:PSS exhibits a broad diffuse reflectance peak at 2θ = 26º, indicating an amorphous character, which is related to the π-π stacking between the amorphous PSS and the chains of PEDOT. The presence of the amorphous PEDOT:PSS can be more effectively interspersed between the neighboring BC layers, which plays a significant role in the facilitation of the stress transfer and the enhancing fracture energy dissipation. Moreover, similar diffraction peaks are observed in PEDOT:PSS/BC composite films, indicating that layer-by-layer assembly has no significant effect in BC crystal structure.

Fig. 2b demonstrates the Fourier transform infrared (FTIR) spectra of BC, PEDOT:PSS, and the PEDOT:PSS/BC composite films. The BC shows a broad absorption band at 3424 cm^{-1} due to the -OH stretching vibration. A relatively weak absorption peak is observed at 2951 cm^{-1} corresponding to the C-H stretching vibration of methyl ($-CH_3$) and methylene ($-CH_2$). At 1619 cm^{-1}, a moderately high absorption peak appears, caused by the corresponding C=O stretching vibration within the cellulose molecule. The absorption peaks

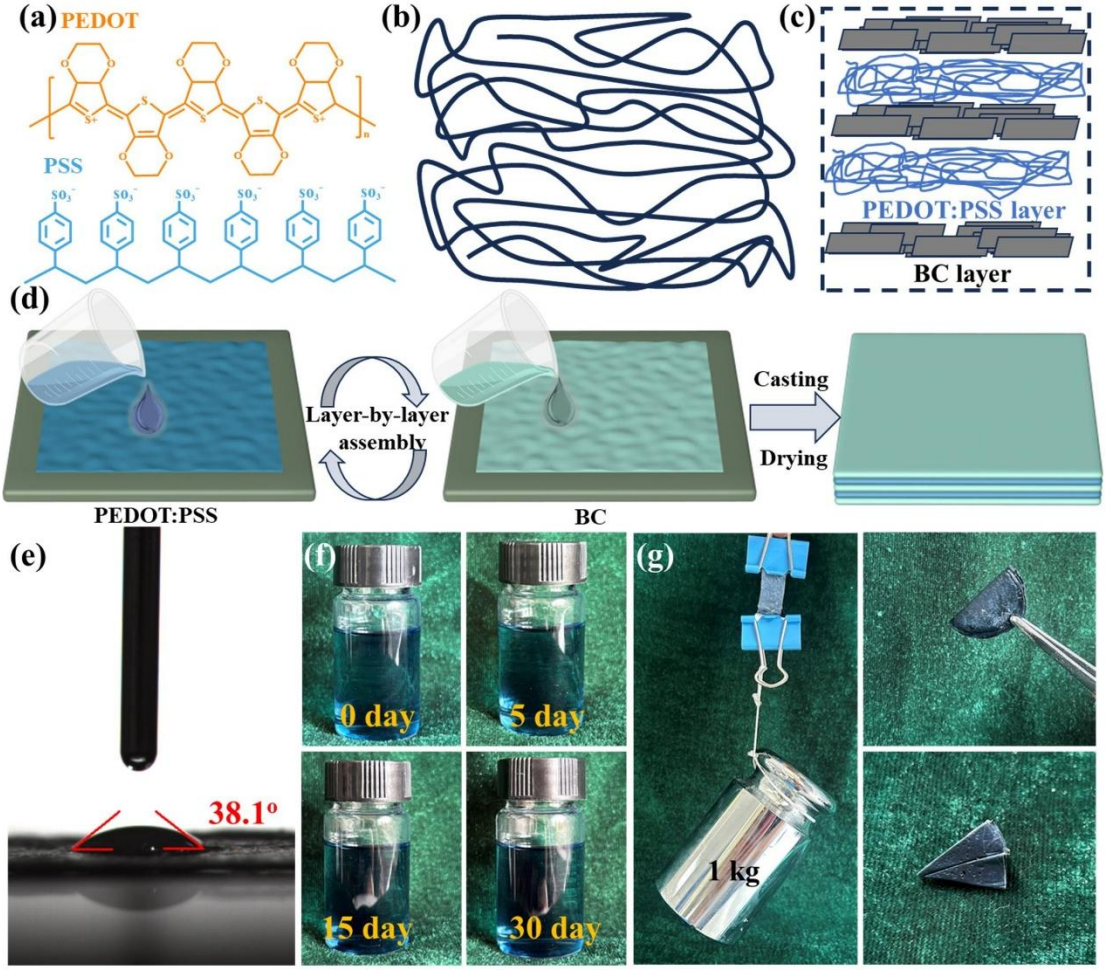

Fig. 1: (a) The structure formula of PEDOT:PSS and (b) structure model of BC. (c) The structure of PEDOT:PSS/BC composite films (d) Schematic diagram for the fabrication and (e) contact angle of the PEDOT:PSS/BC composite films. (f) Digital photos of PEDOT:PSS dispersion and (g) PEDOT:PSS/BC composite films which can withstand a weight of 1kg and possess ultra-flexibility.

at 1337 cm^{-1} and 1121 cm^{-1} correspond to the C-O stretching vibration as well as C-H bending vibration caused by the pyranose ring skeleton oscillation, respectively.[55] In PEDOT:PSS, the absorption peaks correspond to C=C bonds in the thiophene skeleton at 1624 cm^{-1}, while the quasi-substituted peaks of -SO_3 and benzene rings in PSS are found at 1341 cm^{-1}, 1117 cm^{-1} and 780 cm^{-1}.[56]The characteristic peaks of BC and PEDOT:PSS are combined in the PEDOT:PSS composite films. These results indicate that no chemical reactions occurred during evaporation and storage.

To further analyze the chemical compositions in PEDOT:PSS/BC composite films, X-ray photoelectron spectroscopy (XPS) is conducted in Fig. 2c. The peaks at 530.6 eV and 284.7 eV correspond to O 1s and C 1s in BC. In PEDOT:PSS, the peaks at 532.4 eV, 282.8 eV, and 167.1 eV correspond to the characteristic peaks of O 1s, C 1s, and S2p.[57,58] In PEDOT:PSS/BC composite films, the characteristic peak of S 2p appears at 165.2 eV, indicating that the PEDOT:PSS/BC composite films are successfully prepared, which is consistent with the XRD results. In S 2p spectra (Fig. 2d), the peaks at 167.4 eV and 168.7 eV are attributed to the SO_x (x=2,3) group in the PSS, while the peaks at 162.7 eV and 164.1 eV represent the C-S bond in the oxidized thiophene ring.

3.3 Morphologies of PEDOT:PSS/BC composite films

Fig. 3b shows the cross-sectional SEM image of the PEDOT:PSS/BC composite film. The PEDOT:PSS/BC composite film exhibits a distinct layered structure, with layers stacked closely to each other without obvious stratification or penetration. This lays the foundation for PEDOT:PSS/BC composite films with superior electrical insulation. Fig. 3(a, c) shows SEM images of the BC layer and PEDOT:PSS layer, respectively. The BC layer exhibits a connected layer structure, whereas layer PEDOT:PSS has a smooth surface. This is due to the excellent solubility of PEDOT:PSS in water as well as the regular arrangement and aggregation of the PEDOT molecular chains during the drying process.

Figs. 3(d-f) show the energy dispersive X-ray spectroscopy (EDS) distribution of PEDOT:PSS/BC composites film. It illustrates a uniform distribution of C and O elements. The S element, the characteristic of PEDOT:PSS shows a high-density layered distribution, indicating that the PEDOT:PSS polymers are well stacked between the BC layers. The BC layers, at both top and bottom of the multilayered structure, reduce the likelihood electrocution, thereby enhancing

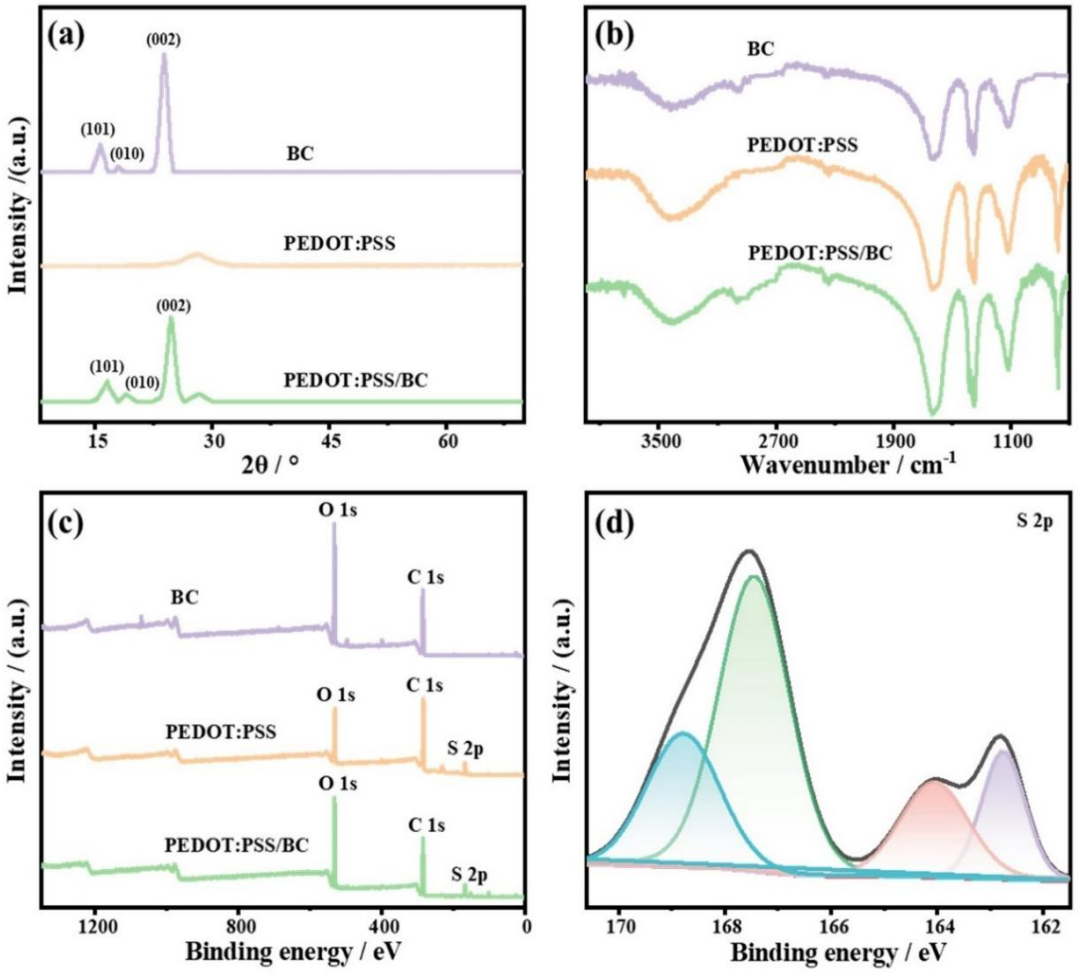

Fig. 2: (a) XRD patterns, (b) FT-IR spectra and (c) XPS spectra for BC, PEDOT:PSS and PEDOT:PSS/BC composite films, and (d) XPS spectra for S 2p of PEDOT:PSS/BC composite films.

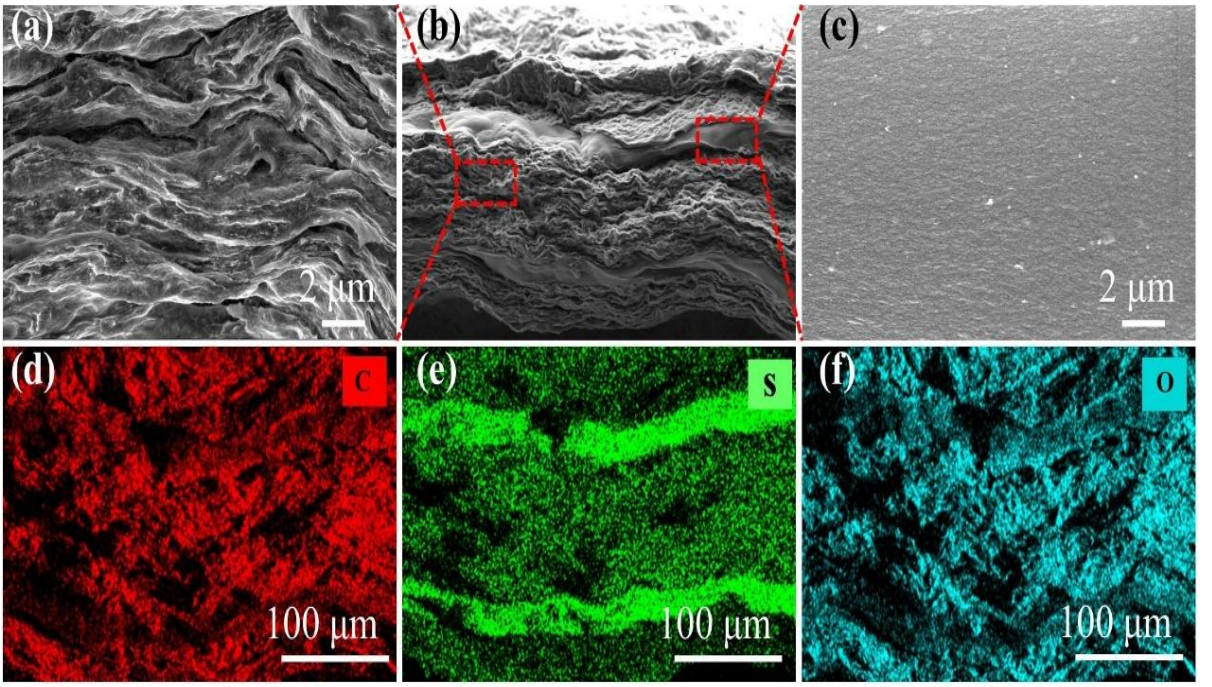

Fig. 3: Cross-sectional SEM images of (b) the PEDOT:PSS/BC film, BC layer (a), PEDOT:PSS layer (c), and corresponding EDS images of (d) C, (e) S, and (f) O elements.

electrical safety. Moreover, the multilayered structure endows PEDOT:PSS/BC composite films with superior mechanical properties, which also promotes the enhancement of the internal multiple reflection and absorption loss of electromagnetic waves (EMW).

3.4 The EMI shielding performance of PEDOT:PSS/BC composite films

Fig. 4a demonstrates the electrical insulation properties of the PEDOT:PSS/BC composite films. The volume resistivity of the pure BC film is 2.3×10^{12} Ω·cm, indicating it is an effective insulator. With increasing mass fractions of PEDOT:PSS, the volume resistivity of PEDOT:PSS/BC composite films exhibits a descending trend, and it decreases from 4.6×10^{7} Ω·cm for the 10 wt% PEDOT:PSS/BC composite film to 2.0×10^{6} Ω·cm for the 50 wt% PEDOT:PSS/BC composite film. This attributed to the inherent electrical conductivity of PEDOT:PSS, which possesses π-π conjugated structure to enhance electron transport. With increasing mass fractions of PEDOT:PSS, more charge carriers will inevitably reduce the volume resistivity. This provides an important basis for evaluating the electrical properties of PEDOT:PSS/BC composite films for use in electronic devices. The BC layer maintains electrical insulation while allowing PEDOT:PSS to retain an independent conductive layer, forming a multilayer structure with external insulation and internal conductivity, thereby providing superior EMI shielding performance. Fig. 4b demonstrates the EMI shielding performance of PEDOT:PSS/BC composite films in the X-band (8.2-12.4 GHz). With increasing mass fractions of PEDOT:PSS, the EMI SE of PEDOT:PSS/BC composite films steadily increases, and it increases from 44 dB for the 10 wt% PEDOT:PSS/BC composite film to 72 dB for the 50 wt% PEDOT:PSS/BC composite film.

Fig. 4c compares the contribution of absorption efficiency (SE_A) and reflection efficiency (SE_R) to the total shielding effectiveness (SE_T) of PEDOT:PSS/BC composite films. With increasing mass fractions of PEDOT:PSS, SE_A has the same trend with SE_T and much larger than SE_R. The SE_A increases from 35 dB for the 10 wt% PEDOT:PSS/BC composite film to 56 dB for the 50 wt% PEDOT:PSS/BC composite film, whereas the SE_R only increases from 9 dB for the 10 wt% PEDOT:PSS/BC composite film to 16 dB for the 50 wt% PEDOT:PSS/BC composite film. When EMW reach the surface of PEDOT:PSS/BC composite films, some of the incident EMW are reflected when they encounter the conductive PEDOT:PSS layer due to impedance mismatch. For the EMW entering the PEDOT:PSS layer, their interaction with a high density of electron carriers (such as electrons, holes, and dipoles) results in a large amount of conductive loss and attenuation of the EMW energy through induced currents. At the same time, multiple internal reflections between neighboring PEDOT:PSS layers promote the dissipation and attenuation of EMW, endowing PEDOT:PSS/BC composite films excellent EMI shielding performance.

Fig. 4d demonstrates the comparison for EMI shielding performance of PEDOT:PSS/BC composite films with recently reported EMI shielding materials, and the corresponding detailed data are provided in Table S1. The EMI SE of the PEDOT:PSS/BC composite film is higher than that of graphene/PEDOT:PSS film (54 dB for 0.02 mm) and MXene/WPU composites (53 dB for 0.035 mm),[59,60] showing superior EMI shielding performance. And the EMI shielding performance and mechanical properties of the PEDOT:PSS

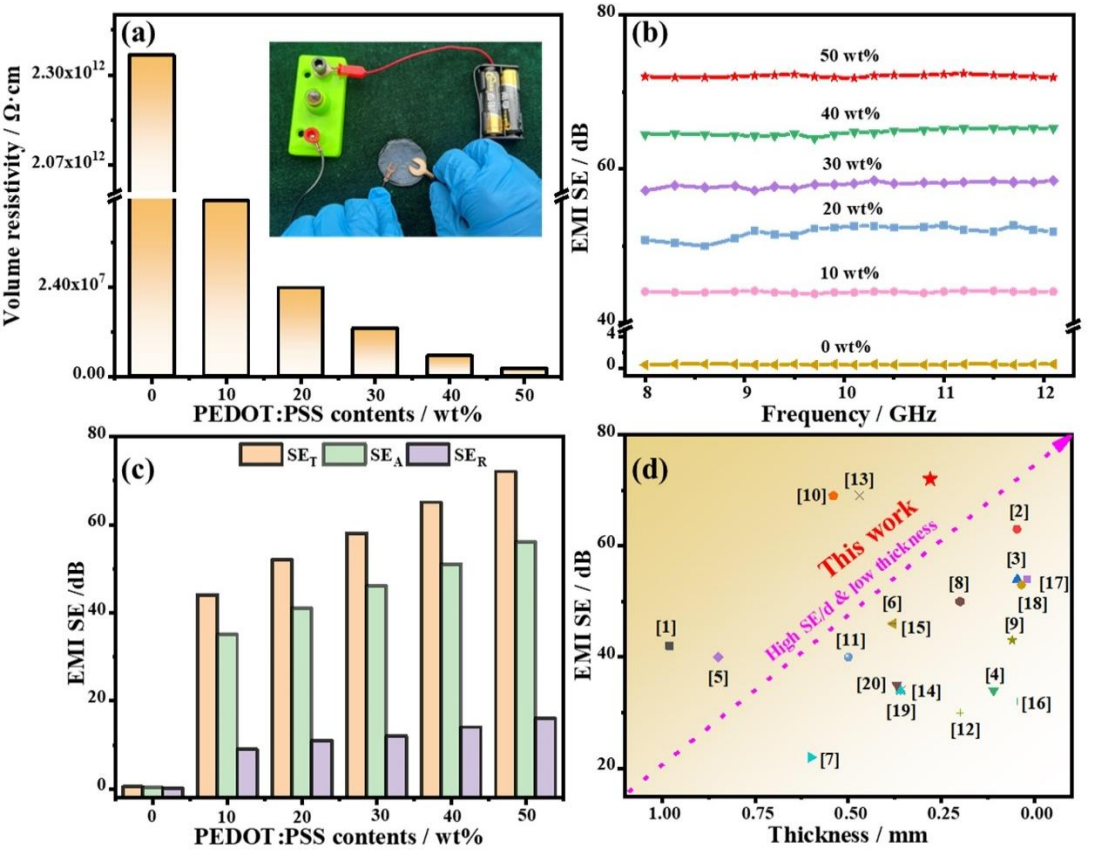

Fig. 4: (a) The volume resistivity of the PEDOT:PSS/BC film. (b) The EMI SE and (c) corresponding SE_T, SE_A, SE_R. (d) EMI SE vs. thickness of PEDOT:PSS/BC composite films compared with other works.

composite films are compared with other reported works (Fig. S1 and Table S2), presenting great potential for industrial applications.

In practical applications, complicated and harsh working environments are great challenges for EMI shielding composites. A series of rigorous environmental experiments are carried out to explore the endurance of PEDOT:PSS/BC composite films for EMI shielding performance. As shown in Fig. 5a, the stable EMI SE of PEDOT:PSS/BC composite films varies after 1000 bending cycles. After cycling, the EMI SE only decreases by about 2 dB, indicating that the EMI shielding performance is extremely stable when resisting mechanical bending. Meanwhile, after immersion in liquid nitrogen for 200 s (Fig. 5b) or baking at 90 °C for 2 h (Fig. 5c) or exposure to air for one month (Fig. 5d), the PEDOT:PSS/BC composite films still maintain high EMI SE, indicating their excellent EMI shielding durability. Fig. 5e demonstrates that the EMI SE of the PEDOT:PSS/BC composite film remains above 69 dB after ultrasonication for 1 h. Therefore, the PEDOT:PSS/BC composite films have superior resistance to extreme environments under mechanical wearing and maintain stable EMI shielding performance under various extreme conditions, which is mainly due to the multilayer structure of PEDOT:PSS/BC composite films. Subsequently, the EMI shielding performance of PEDOT:PSS/BC composite films are tested under strong acidic/alkaline, salt solution, organic solvent, etc., and the EMI SE are almost the same as the initial state. In summary, the superior EMI shielding stability of the PEDOT:PSS/BC composite films imply their great potential for applications in electronic devices operating under harsh conditions. (Fig. 5f).

3.5 Mechanical properties of PEDOT:PSS/BC composite films

Superior mechanical properties are important for the practical applications of EMI shielding materials. Figs. 6a and b show the tensile stress-strain curves and tensile strength and strain of the PEDOT:PSS/BC composite films. The tensile strength of the BC film is 131.9 MPa. With increasing mass fractions of PEDOT:PSS, the tensile strength gradually decreases from 119.0 MPa for the 10 wt% PEDOT:PSS/BC composite film to 62.5 MPa for the 50 wt% PEDOT:PSS/BC composite film, and the strain at break increases from 13.3% to 21.5%. Fig. 6c shows the modulus and toughness of PEDOT:PSS/BC composite films. With increasing mass fractions of PEDOT:PSS, the toughness and modulus gradually decrease from 10.3 MJ/m^3 to 6.6 MJ/m^3 and from 11.1 GPa for the 10 wt% PEDOT:PSS/BC composite film to 3.38 GPa for the 50 wt% PEDOT:PSS/BC composite film. With increasing mass fractions of PEDOT: PSS, too much PEDOT:PSS may form a weaker interfacial layer between the layers. This will reduce the bonding force and the layers are prone to relative sliding or peeling off when subjected to external forces, resulting in a decrease in the mechanical properties of the PEDOT: PSS/BC

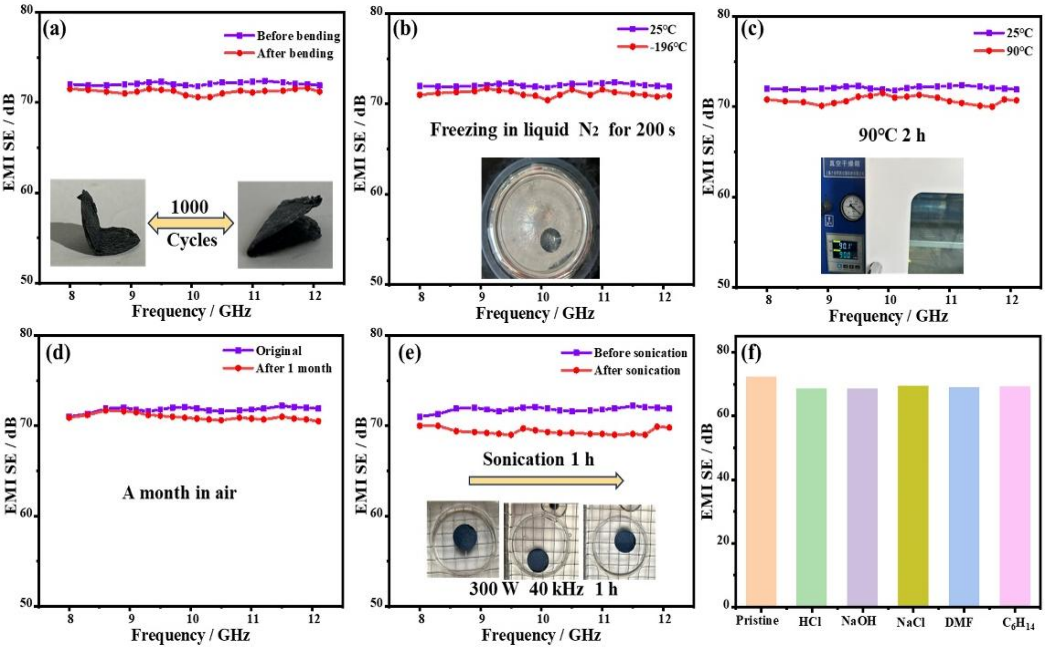

Fig. 5: (a) EMI SE of the PEDOT:PSS/BC film before and after bending. (b) EMI SE of the PEDOT:PSS/BC film before and after treatment at -196 ℃. (c) EMI SE of the PEDOT:PSS/BC film before and after 90 ℃ treatment. (d) EMI SE of the PEDOT:PSS/BC film before and after one month in air. (e) EMI SE of the PEDOT:PSS/BC film before and after ultrasonic cleaning 1 h. (f) Comparison of average total EMI SE of PEDOT:PSS/BC composite films after soaking in various liquids with the pristine ones.

composite films with theincreasing fractions of PEDOT:PSS.

Fig. 6d shows the tensile strength and toughness of PEDOT:PSS/BC composite films after folding for different times. The tensile strength and toughness of PEDOT:PSS/BC composite films are almost unchanged after hundreds or thousands of folds, it still remains 95.7% and 91.2% of the original tensile strength and toughness. This is because the self-supporting nature of the BC layer and PEDOT:PSS layer

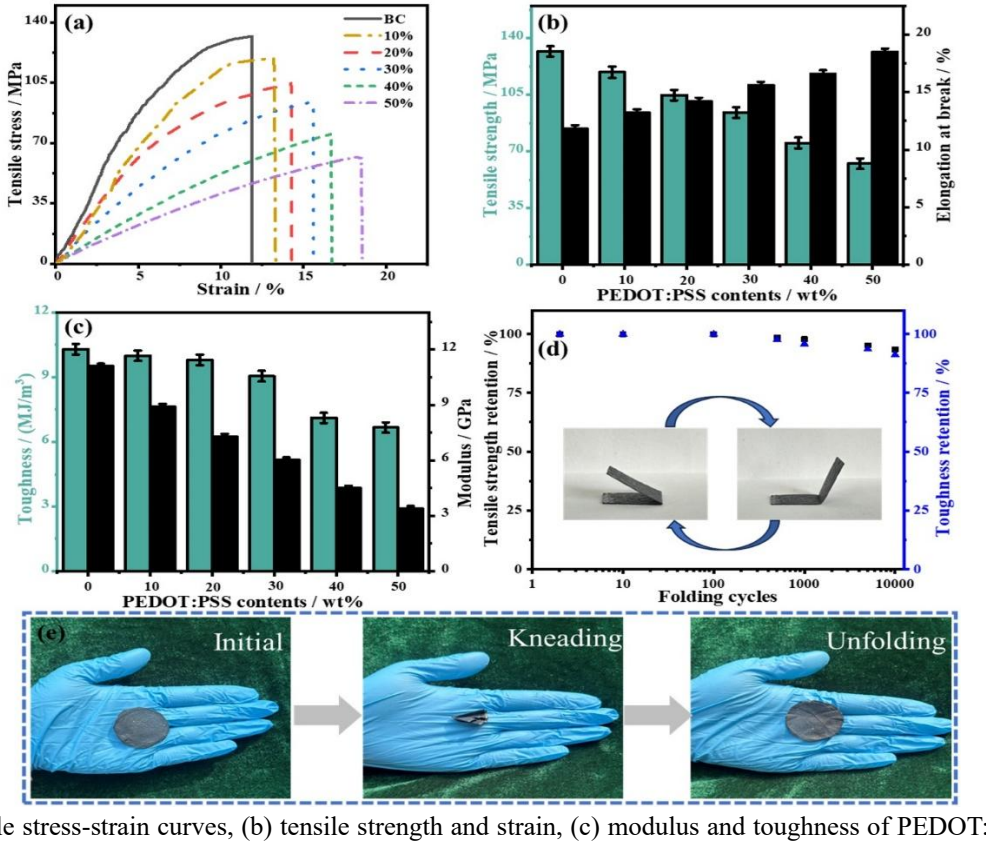

Fig. 6: (a) The tensile stress-strain curves, (b) tensile strength and strain, (c) modulus and toughness of PEDOT:PSS/BC films. (d) Tensile strength and toughness retention of PEDOT:PSS/BC films after repetitive folding. (e) Digital photos of PEDOT:PSS/BC composite films showing excellent folding endurance.

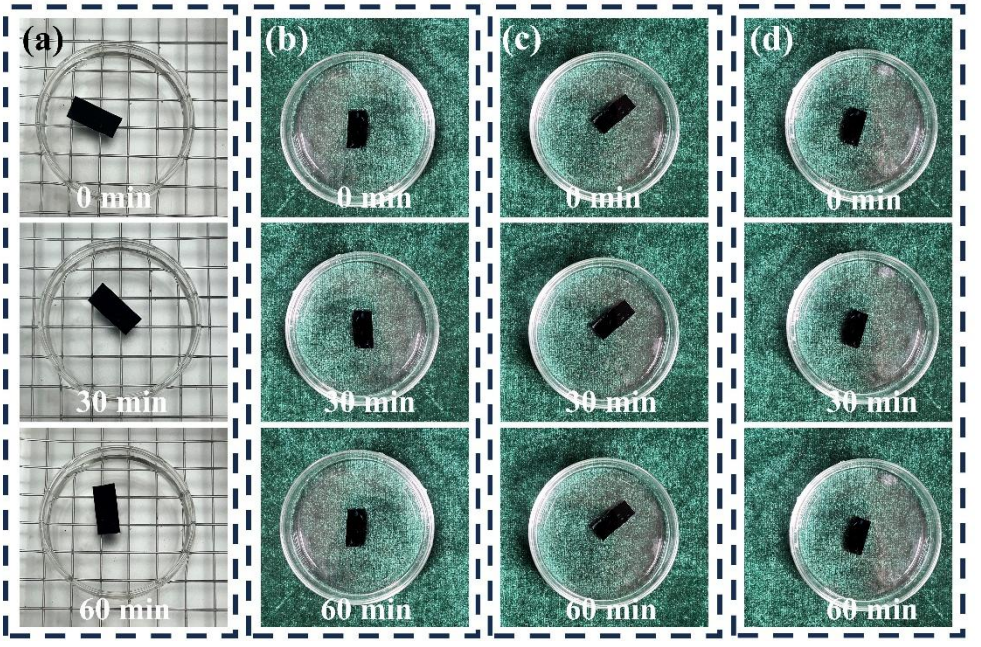

Fig. 7: (a) Digital photos of the PEDOT:PSS/BC film after sonication. (b) Digital photos of the PEDOT:PSS/BC film after soaked in HCl, (b) NaOH, and (c) DMF.

the hydrogen bonding force, and the adhesive force enables the PEDOT:PSS/BC composite films with excellent flexibility and fatigue resistance. In addition, Fig. 6e demonstrates that the PEDOT:PSS/BC composite films can be restored to its original shape intact without any cracks after being kneaded into a ball. This can be attributed to the fact that the PEDOT:PSS/BC composite film forms multilayer structure. This arrangement is crucial for ensuring structural stability and contributing to the overall high tensile stress. Moreover, the multilayer structure plays a pivotal role in enhancing structural robustness and maintaining high tensile stress performance.

3.7 Chemical stability of PEDOT:PSS/BC composite films

To evaluate the structural stability of the composites, ultrasonic testing (300 W, 40 kHz) is conducted on the PEDOT:PSS/BC composite films (Fig. 7a). The results demonstrate that the PEDOT:PSS/BC composite films exhibit superior resistance to ultrasonic waves, with no surface breakage observed after being subjected to ultrasonication for 1 hour. In order to verify the stability of the multilayer structural composites, the harsh environment is simulated by acidic (3 M HCl) (Fig. 7b), alkaline (3 M NaOH) (Fig. 7c), and N, N-Dimethylformamide (DMF) (Fig. 7d) environments. The surface morphology of the PEDOT:PSS/BC composite films are stabilized without corrosion or damage after 1 h. These results indicate that the PEDOT:PSS/BC composite films have superior chemical tolerance in harsh environments.

4. Conclusion

In this work, insulating PEDOT:PSS/BC EMI shielding composite films with excellent mechanical properties and superior flexibility are successfully prepared by layer-by-layer assembly. When the mass fractions of PEDOT:PSS are 50 wt%, the PEDOT:PSS/BC composite films exhibit volume resistivity as high as 2.0×10^{6} Ω·cm and EMI SE of 72 dB in the X-band and they can maintain efficient EMI shielding performance under various harsh conditions (high temperature, low temperature and ultrasonication). In addition, the PEDOT:PSS/BC composite films possess excellent flexibility, mechanical properties, and long-term durability (harsh chemical environments and severe mechanical wearing). This work proposes a facile strategy to design insulating polymer-based EMI shielding composite films with excellent mechanical properties and superior flexibility, which shows great potential for applications in electronic packaging, flexible electronic devices, aeronautics and astronautics.

Acknowledgments

This work was supported by the National Natural Science Foundation of China (52303090); The Innovation Capability Support Plan of Shaanxi Province (2024ZC-KJXX-022); The Youth Talent Promotion Project of Shaanxi Science and Technology Association (20240426); The Special Scientific Research Plan of Education Department of Shaanxi Province (23JK0376). The Postdoctoral Research Project of Shaanxi Province (2024BSHSDZZ010). The authors extend their appreciation to the Deanship of Scientific Research at Northern Border University, Arar, KSA, for funding this research work through the project number NBU-FFR-2025-2193-13. The authors would like to thank Shiyanjia Lab (www.shiyanjia.com) for supporting SEM tests.

Conflict of Interest

There is no conflict of interest.

Supporting Information

Applicable.

References

[1] H. Lv, Z. Yang, H. Pan, R. Wu, Electromagnetic absorption materials: Current progress and new frontiers, *Progress in Materials Science*, 2022, **127**, 100946, doi: 10.1016/j.pmatsci.2022.100946.

[2] Y. Xia, W. Gao, C. Gao, A review on graphene-based electromagnetic functional materials: electromagnetic wave shielding and absorption, *Advanced Functional Materials*, 2022, **32**, 2204591, doi: 10.1002/adfm.202204591.

[3] J. Yan, T. Zhou, X. Yang, Z. Zhang, L. Li, Z. Zou, Z. Fu, Q. Cheng, Strong and tough MXene bridging-induced conductive nacre, *Angewandte Chemie International Edition*, 2024, **63**, e202405228, doi: 10.1002/anie.202405228.

[4] C. Xiong, Q. Xiong, M. Zhao, B. Wang, L. Dai, Y. Ni, Recent advances in non-biomass and biomass-based electromagnetic shielding materials, *Advanced Composites and Hybrid Materials*, 2023, **6**, 205, doi: 10.1007/s42114-023-00774-6.

[5 Z. Ma, H. Qiu, Y. Zhang, Z. Yu, J. Gu, Significantly enhanced electromagnetic interference shielding performances of epoxy nanocomposites with long-range aligned lamellar structures, *Nano-Micro Letters*, 2022, **14**, 224, doi: 10.1007/s40820-022-00949-8.

[6] L. Wang, J. Cheng, Y. Zou, W. Zheng, Y. Wang, Y. Liu, H. Zhang, D. Zhang, X. Ji, Current advances and future perspectives of MXene-based electromagnetic interference shielding materials, *Advanced Composites and Hybrid Materials*, 2023, **6**, 172, doi: 10.1007/s42114-023-00752-y.

[7] Z. Ma, R. Jiang, J. Jing, S. Kang, L. Ma, K. Zhang, J. Li, Y. Zhang, J. Qin, S. Yun, G. Zhang, Lightweight dual-functional segregated nanocomposite foams for integrated infrared stealth and absorption-dominant electromagnetic interference shielding, *Nano-Micro Letters*, 2024, **16**, 223, doi: 10.1007/s40820-024-01450-0.

[8] L. Lang, Y. Zou, Y. Wang, J. Men, J. Cheng, X. Yan, J. Zhu, Y. Liu, S. Zhang, Z. Li, X. Ji, L. Wang, A review of recent advances in MXenes/polymer-based electromagnetic interference shielding materials, *Polymer Composites*, 2024, **45**, 11541-11559, doi: 10.1002/pc.28627.

[9] L. Wang, P. Song, C. Lin, J. Kong, J. Gu, 3D shapeable, superior electrically conductive cellulose nanofibers/$Ti_3C_2T_x$MXene aerogels/epoxy nanocomposites for promising EMI shielding, *Research*, 2020, **2020**, 1-12, doi: 10.34133/2020/4093732.

[10] J. Chang, H. Zhai, Z. Hu, J. Li, Ultra-thin metal composites for electromagnetic interference shielding, *Composites Part B: Engineering*, 2022, **246**, 110269, doi: 10.1016/j.compositesb.2022.110269.

[11] R. B. Jagadeesh Chandra, B. Shivamurthy, S. B. Bore Gowda, M. Sathish kumar, Flexible linear low-density polyethylene laminated aluminum and nickel foil composite tapes for electromagnetic interference shielding, *Engineered Science*, 2023, **21**, 777, doi: 10.30919/es8d777.

[12] C. Wang, W. Li, K. Wang, R. Xue, X. Liu, S. Zhou, Z. Zhao, Dual three-dimensional ultra-flexible polymer-based phase change composite materials for body hyperthermia therapy: Ultra-low leakage rate, high thermal conductivity, and photothermal conversion efficiency, *Journal of Energy Storage*, 2025, **118**, 116175, doi: 10.1016/j.est.2025.116175.

[13] L. Wang, Z. Ma, Y. Zhang, L. Chen, D. Cao, J. Gu, Polymer-based EMI shielding composites with 3D conductive networks: A mini-review, *SusMat*, 2021, **1**, 413-431, doi: 10.1002/sus2.21.

[14] W. Zou, X. Zheng, J. Huang, G. Wang, Z. Guo, Recent advances in injection molding of carbon fiber reinforced thermoplastic polymer composites: a review, *ES General*, 2023, **1**, 938, doi: 10.30919/esg938.

[15] R. S. Desai, R. S. Desai, V. S. Jadhav, P. S. Patil, D. S. Dalavi, Electrodeposition of polyaniline nanoparticles as high-performance electrode for supercapacitor application, *ES General*, 2024, **6**, 1255, doi: 10.30919/esg1255.

[16] X. Xu, Y. Wang, C. Wang, B. Cui, C. Wang, Multifunctional C/TiO_2 from MXene/polyaniline for electromagnetic protection and supercapacitor, *Energy Material Advances*, 2024, **5**, 70, doi: 10.34133/energymatadv.0070.

[17] Z. Han, Y. Niu, X. Shi, D. Pan, H. Liu, H. Qiu, W. Chen, B. B. Xu, Z. M. El-Bahy, H. Hou, E. R. Elsharkawy, M. A. Amin, C. Liu, Z. Guo, MXene@c-MWCNT adhesive silica nanofiber membranes enhancing electromagnetic interference shielding and thermal insulation performance in extreme environments, *Nano-Micro Letters*, 2024, **16**, 195, doi: 10.1007/s40820-024-01398-1.

[18] Y. Bai, J. Ju, Y. Pan, B. Zhang, D. Wang, X. Li, Flexible multifunctional composite films for adjustable EMI shielding behavior under self-fixed deformation, *Chemical Engineering Journal*, 2024, **500**, 156896, doi: 10.1016/j.cej.2024.156896.

[19] F. Jia, Z. Lu, T. Huang, M. Xu, X. Xu, Z. Guo, S. Wang, J. Dong, Y. Kou, L. Hua, Twin-coated skeleton PEDOT: PSS/MXene/Para-aramid nanofibers hybrid aerogel with efficient EMI shielding performance and tunable power coefficient, *Advanced Composites and Hybrid Materials*, 2025, **8**, 200, doi: 10.1007/s42114-025-01290-5.

[20] J. Feng, Z. Zhuang, Y. Zhou, C. Li, Highly conductive PEDOT: PSS aerogels, *Advanced Functional Materials*, 2024, **34**, 2315188, doi: 10.1002/adfm.202315188.

[21] G. Chang, L. Zeng, L. Xie, B. Xue, Q. Zheng, Ultrathin multifunctional electromagnetic interference shielding MXene/AgNWs/PEDOT: PSS coatings with superior electro/photo-thermal transition ability and water repellency, *Chemical Engineering Journal*, 2023, **470**, 144033, doi: 10.1016/j.cej.2023.144033.

[22] G. K. Sharma, S. L. Joseph, N. R. James, Recent progress in poly (3, 4-ethylene dioxythiophene): polystyrene sulfonate based composite materials for electromagnetic interference shielding, *Advanced Materials Technologies*, 2024, **9**, 2301203, doi: 10.1002/admt.202301203.

[23] J. Zhou, Y. Zhu, K. Qian, M. Miao, X. Feng, Poly(3, 4-ethylenedioxythiophene): sulfamic acid modified aramid nanofibers: an innovative conductive polymer with enhanced electromagnetic interference shielding and thermoelectric

performance, *Small*, 2024, **20**, 2405400, doi: 10.1002/smll.202405400.
[24] J. Wu, H. Xie, C. Fang, C. Ji, G. Zhang, Y. Lin, Y. Pei, X. Zhan, L. Ma, MWCNT-promoted PEDOT: PSS in polyurethane films: enhancing conductivity and EMI shielding, *Surfaces and Interfaces*, 2025, **62**, 106265, doi: 10.1016/j.surfin.2025.106265.
[25] N. Keshmiri, A. H. Ahmadian Hoseini, P. Najmi, J. Liu, A. S. Milani, M. Arjmand, Highly conductive polystyrene/carbon nanotube/PEDOT: PSS nanocomposite with segregated structure for electromagnetic interference shielding, *Carbon*, 2023, **212**, 118104, doi: 10.1016/j.carbon.2023.118104.
[26] P. J. Bora, A. G. Anil, K. J. Vinoy, P. C. Ramamurthy, Outstanding absolute electromagnetic interference shielding effectiveness of cross-linked PEDOT: PSS film, *Advanced Materials Interfaces*, 2019, **6**, 1901353, doi: 10.1002/admi.201901353.
[27] D. Guo, C. Mu, Q. Liu, B. Wang, J. Xiang, A. Nie, K. Zhai, Y. Shu, T. Xue, F. Wen, Z. Liu, Aramid nanofiber/polypyrrole composite films for broadband EMI shielding, wearable electronics, joule heating, and photothermal conversion, *ACS Applied Nano Materials*, 2023, **6**, 15108-15118, doi: 10.1021/acsanm.3c02645.
[28] G. Chu, Z. Nie, Y. Peng, H. Xu, X. Yang, X. Guo, M. Jiang, F. Dong, Z. Guo, S. Qi, J. Zhang, Spin-coating ANF based multilayer symmetric composite films for enhanced electromagnetic interference shielding and thermal management, *Journal of Colloid and Interface Science*, 2025, **679**, 521-530, doi: 10.1016/j.jcis.2024.09.248.
[29] Y. Zhang, Z. Ma, K. Ruan, J. Gu, Flexible $Ti_3C_2T_x$/(aramid nanofiber/PVA) composite films for superior electromagnetic interference shielding, *Research*, 2022, **2022**, 1-12, doi: 10.34133/2022/9780290.
[30] C. Wang, Z. Zhao, S. Zhou, L. Wang, X. Liu, R. Xue, Facile fabrication of densely packed ammoniated alumina/MXene/bacterial cellulose composite films for enhancing thermal conductivity and photothermal conversion performance, *Journal of Materials Science & Technology*, 2025, **213**, 162-173, doi: 10.1016/j.jmst.2024.06.024.
[31] L. Tang, Q. Hu, X. Pan, Y. Lei, L. Li, Y. Wang, W. Zhou, J. Liu, J. Zhang, X. Liu, Surface modification of PBO fibers with random copolymer containing benzoxazole for improving surface activity, and enhancing interfacial bonding strength with cyanate ester resins, *Advanced Composites and Hybrid Materials*, 2024, **8**, 41, doi: 10.1007/s42114-024-01119-7.
[32] J. Jiang, P. Zhou, Y. Yi, D. Chen, G. Hu, X. Liu, L. Tang, Dual-crosslinked network structured polybenzoxazine/PBO nanofiber aerogel with thermal insulation, flame retardancy, and super-hydrophobicity, *Polymer Degradation and Stability*, 2025, **234**, 111216, doi: 10.1016/j.polymdegradstab.2025.111216.
[33] A. Liu, H. Qiu, X. Lu, H. Guo, J. Hu, C. Liang, M. He, Z. Yu, Y. Zhang, J. Kong, J. Gu, Asymmetric structural MXene/PBO aerogels for high-performance electromagnetic interference shielding with ultra-low reflection, *Advanced Materials*, 2025, **37**, 2414085, doi: 10.1002/adma.202414085.
[34] A. Isogai, T. Saito, H. Fukuzumi, TEMPO-oxidized cellulose nanofibers, *Nanoscale*, 2011, **3**, 71-85, doi: 10.1039/C0NR00583E.
[35] L. Wang, L. Lang, X. Hu, T. Gao, M. He, H. Qiu, X. Ji, H. Guo, Y. Zhang, S. Huang, Multifunctional ionic bonding-strengthened (Ti3C2T MXene/CNF)-(BNNS/CNF) composite films with Janus structure for outstanding electromagnetic interference shielding and thermal management, *Journal of Materials Science & Technology*, 2025, **224**, 46-55, doi: 10.1016/j.jmst.2024.11.010.
[36] C. Xiong, C. Zheng, Z. Zhang, Q. Xiong, Q. Zhou, D. Li, M. Shen, Y. Ni, Polyaniline@cellulose nanofibers multifunctional composite material for supercapacitors, electromagnetic interference shielding and sensing, *Journal of Materiomics*, 2025, **11**, 100841, doi: 10.1016/j.jmat.2024.01.015.
[37] L. Wang, Z. Yang, L. Lang, J. Men, T. Gao, Q. Wang, J. Cheng, Y. Liu, N. Zheng, J. Liu, X. Ji, Flexible multifunctional MXene/polyimide films with Janus structure for superior electromagnetic interference shielding, *Advanced Composites and Hybrid Materials*, 2024, **8**, 26, doi: 10.1007/s42114-024-01100-4.
[38] B. Zhou, J. Song, B. Wang, Y. Feng, C. Liu, C. Shen, Robust double-layered ANF/MXene-PEDOT: PSS Janus films with excellent multi-source driven heating and electromagnetic interference shielding properties, *Nano Research*, 2022, **15**, 9520-9530, doi: 10.1007/s12274-022-4756-x.
[39] X. Liu, L. Tian, Z. Bao, Y. Zhang, P. Qian, W. Geng, D. Zhang, Q. Zhu, H. Geng, Caffeic-acid-functionalized MWCNTs and PEDOT: PSS formed composite flexible films with "reinforced concrete" structure for electrical heating and EMI shielding, *ACS Applied Materials & Interfaces*, 2024, **16**, 22391-22402, doi: 10.1021/acsami.4c01373.
[40] C. Luo, M. Huang, C. Sun, K. Zhao, H. Guo, M. Wang, Anisotropic electromagnetic wave shielding performance in Janus cellulose nanofiber composite films, *Materials Today Physics*, 2024, **44**, 101440, doi: 10.1016/j.mtphys.2024.101440.
[41] Z. Nan, W. Wei, Z. Lin, J. Ouyang, J. Chang, Y. Hao, Flexible electromagnetic interference shields: Materials, structure and multifunctionalization, *Materials Science and Engineering: R: Reports*, 2024, **160**, 100823, doi: 10.1016/j.mser.2024.100823.
[42] Y. Fan, Y. Wang, J. Qiu, Multifunctional thermal interface composites with enhanced thermal conductivity, EMI shielding capabilities, and mechanical performance, *Composites Communications*, 2024, **51**, 102116, doi: 10.1016/j.coco.2024.102116.
[43] Z. Ma, Y. Zhang, R. Jiang, L. Shao, J. Cao, H. Guo, G. Zhang, Highly stretchable and room-temperature self-healing sheath-core structured composite fibers for ultrasensitive strain sensing and visual thermal management, *Composites Science and Technology*, 2024, **248**, 110460, doi: 10.1016/j.compscitech.2024.110460.
[44] J. Yun, J. Lee, J. Kim, J. Lee, W. Choi, Hexagonal boron nitride nanosheets/graphene nanoplatelets/cellulose nanofibers-based multifunctional thermal interface materials enabling electromagnetic interference shielding and electrical insulation, *Carbon*, 2024, **228**, 119397, doi: 10.1016/j.carbon.2024.119397.

[45] H. Liu, R. Fu, X. Su, B. Wu, H. Wang, Y. Xu, X. Liu, Electrical insulating MXene/PDMS/BN composite with enhanced thermal conductivity for electromagnetic shielding application, *Composites Communications*, 2021, **23**, 100593, doi: 10.1016/j.coco.2020.100593.
[46] P. Zhang, R. Tian, X. Zhang, X. Ding, Y. Wang, C. Xiao, K. Zheng, X. Liu, L. Chen, X. Tian, Electromagnetic interference shielding epoxy composites with satisfactory thermal conductivity and electrical insulation performance enabled by low-melting-point alloy layered structure, *Composites Part B: Engineering*, 2022, **232**, 109611, doi: 10.1016/j.compositesb.2022.109611.
[47] X. Zhou, P. Min, Y. Liu, M. Jin, Z. Yu, H. Zhang, Insulating electromagnetic-shielding silicone compound enables direct potting electronics, *Science*, 2024, **385**, 1205-1210, doi: 10.1126/science.adp6581.
[48] L. Li, Y. Yan, J. Liang, J. Zhao, C. Lyu, H. Zhai, X. Wu, G. Wang, Wearable EMI shielding composite films with integrated optimization of electrical safety, biosafety and thermal safety, *Advanced Science*, 2024, **11**, 2400887, doi: 10.1002/advs.202400887.
[49] L. Wang, Z. Ma, Y. Zhang, H. Qiu, K. Ruan, J. Gu, Mechanically strong and folding-endurance $Ti_3C_2T_x$ MXene/PBO nanofiber films for efficient electromagnetic interference shielding and thermal management, *Carbon Energy*, 2022, **4**, 200-210, doi: 10.1002/cey2.174.
[50] Y. Wan, P. Xiong, J. Liu, F. Feng, X. Xun, F. M. Gama, Q. Zhang, F. Yao, Z. Yang, H. Luo, Y. Xu, Ultrathin, strong, and highly flexible $Ti_3C_2T_x$ MXene/bacterial cellulose composite films for high-performance electromagnetic interference shielding, *ACS Nano*, 2021, **15**, 8439-8449, doi: 10.1021/acsnano.0c10666.
[51] B. O. O. Boni, L. Lamboni, B. M. Bakadia, S. A. Hussein, G. Yang, Combining silk sericin and surface micropatterns in bacterial cellulose dressings to control fibrosis and enhance wound healing, *Engineered Science*, 2020, **10**, 68-77, doi: 10.30919/es8d906.
[52] Y. Yang, L. Shao, J. Wang, Z. Ji, T. Zhang, M. Wu, Y. He, C. Wang, J. Ma, An asymmetric layer structure enables robust multifunctional wearable bacterial cellulose composite film with excellent electrothermal/photothermal and EMI shielding performance, *Small*, 2024, **20**, 2308514, doi: 10.1002/smll.202308514.
[53] S. Luo, Q. Li, Y. Xue, B. Zhou, Y. Feng, C. Liu, Reinforcing and toughening bacterial cellulose/MXene films assisted by interfacial multiple cross-linking for electromagnetic interference shielding and photothermal response, *Journal of Colloid and Interface Science*, 2023, **652**, 1645-1652, doi: 10.1016/j.jcis.2023.08.177.
[54] A. Prilepskii, V. Nikolaev, A. Klaving, Conductive bacterial cellulose: From drug delivery to flexible electronics, *Carbohydrate Polymers*, 2023, **313**, 120850, doi: 10.1016/j.carbpol.2023.120850.
[55] Z. Shen, W. Zhu, Y. Huang, J. Zhang, Y. Wu, Y. Pan, G. Yang, D. Wang, Y. Li, B. Z. Tang, Visual multifunctional aggregation-induced emission-based bacterial cellulose for killing of multidrug-resistant bacteria, *Advanced Healthcare Materials*, 2023, **12**, 2300045, doi: 10.1002/adhm.202300045.
[56] S. Tu, T. Tian, T. Xiao, X. Yao, S. Shen, Y. Wu, Y. Liu, Z. Bing, K. Huang, A. Knoll, S. Yin, S. Liang, J. E. Heger, G. Pan, M. Schwartzkopf, S. V. Roth, P. Müller-Buschbaum, Humidity stable thermoelectric hybrid materials toward a self-powered triple sensing system, *Advanced Functional Materials*, 2024, **34**, 2316088, doi: 10.1002/adfm.202316088.
[57] P. Guo, J. Dong, C. Xu, Y. Yao, J. You, H. Bian, W. Zeng, G. Zhou, X. He, M. Wang, X. Zhou, M. Wang, Q. Song, Fabrication of an ultrathin PEG-modified PEDOT: PSS HTL for high-efficiency Sn–Pb perovskite solar cells by an eco-friendly solvent etching technique, *Journal of Materials Chemistry A*, 2023, **11**, 7246-7255, doi: 10.1039/d3ta00455d.
[58] F. Meng, J. Wen, J. Ma, Y. Tian, A dual-functional sensor based on PEDOT: PSS for sensing temperature and ammonia fabricated by electrohydrodynamic printing, *Journal of Materials Science: Materials in Electronics*, 2024, **35**, 1834, doi: 10.1007/s10854-024-13555-8.
[59] Z. Lei, W. Liu, W. Xing, Y. Zhang, Y. Liu, P. Tao, W. Shang, B. Fu, C. Song, T. Deng, Developing thermal regulating and electromagnetic shielding nacre-inspired graphene-conjugated conducting polymer film *via* apparent wiedemann–franz law, *ACS Applied Materials & Interfaces*, 2022, **14**, 49199-49211, doi: 10.1021/acsami.2c14805.
[60] Z. Wang, L. Wang, R. Chang, M. Shi, D. Sun, Construction of alternating multilayer MXene/WPU thin films with excellent EMI shielding performance and mechanical properties, *Journal of Alloys and Compounds*, 2023, **956**, 170367, doi: 10.1016/j.jallcom.2023.170367.